Journal of Theoretical Biology 454 (2018) 60–69

Contents lists available at ScienceDirect

Journal of Theoretical Biology

journal homepage: www.elsevier.com/locate/jtbi

Nuclear apoptotic volume decrease in individual cells: Confocal microscopy imaging and kinetic modeling

Irina V. Khalo[a], Anastasiya I. Konokhova[a], Darya Y. Orlova[c], Konstantin V. Trusov[a,b], Maxim A. Yurkin[a,b], Eva Bartova[d], Stanislav Kozubek[d], Valeri P. Maltsev[a,b,e], Andrei V. Chernyshev[a,b,*]

[a] Voevodsky Institute of Chemical Kinetics and Combustion, Institutskaya 3, Novosibirsk 630090, Russia
[b] Novosibirsk State University, Pirogova 2, Novosibirsk 630090, Russia
[c] Department of Genetics, Stanford University, Campus Drive 279, Stanford, CA 94305, USA
[d] Institute of Biophysics, Academy of Sciences of the Czech Republic, v.v.i., Kralovopolska 135, Brno CZ-612 65, Czech Republic
[e] Novosibirsk State Medical University, Krasny Prospect 52, Novosibirsk 630091, Russia

ARTICLE INFO

Article history:
Received 18 October 2016
Revised 13 May 2018
Accepted 28 May 2018
Available online 30 May 2018

Keywords:
Apoptosis
Nuclear volume decrease
Chromatin condensation
Apoptotic ring
3D time lapsed confocal microscopy
Live cell analysis
Kinetics
Mathematical modeling

ABSTRACT

The dynamics of nuclear morphology changes during apoptosis remains poorly investigated and understood. Using 3D time-lapse confocal microscopy we performed a study of early-stage apoptotic nuclear morphological changes induced by etoposide in single living HepG2 cells. These observations provide a definitive evidence that nuclear apoptotic volume decrease (AVD) is occurring simultaneously with peripheral chromatin condensation (so called "apoptotic ring"). In order to describe quantitatively the dynamics of nuclear morphological changes in the early stage of apoptosis we suggest a general molecular kinetic model, which fits well the obtained experimental data in our study. Results of this work may clarify molecular mechanisms of nuclear morphology changes during apoptosis.

1. Introduction

Apoptosis is an evolutionarily conserved type of programmed cell death initially recognized due to characteristically altered cell morphology (Kerr et al., 1972; Wyllie et al., 1980) and later associated with a variety of biochemical marks (Saraste and Pulkki, 2000; Williams et al., 1974). Successful initiation and execution of tightly regulated apoptotic program depends on activation of genetically controlled pathways mediated by a number of molecular participants from different cellular compartments and is reflected by yielding characteristic morphological and biochemical alterations that are mainly evident in the nucleus (Martelli et al., 2001; Robertson et al., 2000). The dynamics of nuclear morphology changes during apoptosis and mechanisms of apoptotic volume decrease (AVD) remain poorly investigated and understood. Even today, despite a large array of available biochemical assays (Willingham, 1999), easily observable nuclear morphological changes, including chromatin condensation and nuclear shrinkage (nuclear AVD), remain the most reliable, recognizable and, nonetheless, the least studied apoptotic markers.

The dynamics of cellular morphology no less than biochemical alterations represent key apoptotic events and may serve as essential characteristic of apoptotic execution (Pantic et al., 2012; Tone et al., 2007). It is established that nuclear apoptotic program preceding final nuclear collapse/disassembly and formation of apoptotic bodies is executed at least in two consequent stages: early stage I, described by partial chromatin condensation mostly around the nuclear membrane and high-molecular weight DNA cleavage; and stage II, characterized by further chromatin condensation into discrete masses and accompanied by low-molecular weight or oligonucleosomal DNA degradation (Susin et al., 2000; Tone et al., 2007). However these nuclear processes are much more elucidated from biochemical point of view (Yuste et al., 2005). Current knowledge on nuclear apoptotic morphology remains largely qualitative and descriptive. In particular, this applies to early stage of nuclear apoptosis that attracts special attention due to its possibility to

* Corresponding author at: Institute of Chemical Kinetics and Combustion, Institutskaya 3, Novosibirsk 630090, Russia.
E-mail address: chern@kinetics.nsc.ru (A.V. Chernyshev).

https://doi.org/10.1016/j.jtbi.2018.05.034
0022-5193/

be involved in the "decision-making" commitment to cell killing (Samejima and Earnshaw, 2005). There is still no general mechanism proposed to describe nuclear shrinkage despite its seemingly obvious connection with chromatin condensation. The latter in its turn is considered a passive process resulting from the loss of chromatin and DNA structural integrity (Hendzel et al., 1998) and from changes in histone-DNA interactions (Allera et al., 1997). However remarkably little is known about the factors causing these structural changes. There are at least two redundant pathways leading to chromatin condensation and degradation (Susin et al., 2000).

The first caspase-independent pathway induces stage I of nuclear apoptosis and involves apoptosis-inducing factor AIF (Hangen et al., 2010; Loo et al., 2002; Maté et al., 2002; Sevrioukova, 2011; Susin et al., 1999), – the mammalian mitochondrial protein identified as a 57 kDa flavoprotein. The following supposed mechanism (Joza et al., 2009; Loo et al., 2002; Oberhammer et al., 1993; Susin et al., 1999) can be initiated either by a physical stimulus (e.g., noise exposure (Han et al., 2006) or UV-treatment (Pantic et al., 2012)) or a chemical agent (e.g., etoposide (Candé et al., 2002)). In healthy cells, AIF is located in the mitochondrial intermembrane space. During a certain time after the apoptosis initiation mitochondria still retain their integrity while swelling (this stage may be considered as a "lag phase") until the mitochondrial outer membrane becomes ruptured (Han et al., 2006; Sesso et al., 2012; Sun et al., 2007), which leads to AIF exiting into the cytosol. Such mechanism explains the experimentally observed (Bhola et al., 2009) stepwise dynamics (i.e. with the delay time after the stimulation) of the initial stage of the apoptosis. It is also reflected in the corresponding stepwise kinetics of AIF appearance in cytosol near the nucleus. From cytosol AIF translocates into the nucleus and promotes chromatin condensation supposedly through direct binding with the DNA (Artus et al., 2010; Hangen et al., 2015; Maté et al., 2002; Sevrioukova, 2011; Susin et al., 1999; Ye et al., 2002) that occurs prior to the large-scale DNA degradation. The detailed molecular mechanism whereby AIF mediates apoptotic functions in a caspase-independent way remains unclear. AIF, however, is not the only supposed apoptotic effector, which releases from the ruptured mitochondria. Another apoptotic mitochondrial factor is 30 kDa protein endonuclease G (Li et al., 2001; Loo et al., 2002). Although originally identified as a protein involved in mitochondrial DNA replication, endonuclease G was later shown to be released (together with AIF) from mitochondria during apoptosis and to translocate to the cell nucleus, where it is involved in nuclear DNA breakdown (Patterson et al., 1997). The role of endonuclease G in apoptosis is far from being completely understood. Endonuclease-G-induced DNA degradation was shown to be independent of caspase activation, as is also the case for AIF. However, AIF is not a self-nuclease while endonuclease G is. Probably, endonuclease G alone is not sufficient, but requires other nucleases or cofactors. It is possible that both proteins (AIF and endonuclease G) do not act in isolation but require each other for full activity (Han et al., 2006).

The second pathway involving caspases is required for late-apoptosis chromatin condensation and DNA cleavage. However, these pathways are likely to occur in parallel or even activate each other, and importance or order of activation of involved molecules probably depend on cell type and apoptotic stimulus (Candé et al., 2004). These open questions and remaining issues raise a clear need for single-cell analysis methods allowing rigorous quantitative characterization of nuclear-apoptotic-dynamics mechanism and considering individual cellular response. Nuclear apoptosis analysis is still predominantly tackled using population-based assays, using gene knockouts or treating inhibitors (Susin et al., 2000; Tone et al., 2007; Widlak et al., 2002), which provide at their best a relative quantification of nuclei which exhibit a set of particular hallmarks or relative changes in signal intensities.

Such approaches do not provide sufficient temporal and spatial resolution necessary for quantification of nuclear shape and chromatin structure changes on single-cell level. Thus, there is a vital need for methodology for detailed quantification of single-nucleus apoptotic dynamics, based on time-resolved assessment of volume and degree of chromatin condensation and nuclear shrinkage with an emphasis to the sequence and timing of these key stages of nuclear apoptotic program. That also implies a development of mathematical molecular-kinetic models, which are consistent with observable dynamics of nuclear morphological alterations and characterize them by a number of parameters. Such an enhanced approach would be significant from both basic research and clinical perspectives, e.g. in analysis of tumor cell sensitivity to a proapoptotic stimulus or drug.

We try to satisfy this methodological need by presenting an integrated method for the detailed quantitative analysis of the dynamics of early apoptotic nuclear morphological changes. Using time-lapse 3D confocal microscopy of living individual cells in apoptosis we developed a molecular kinetic model of peripheral chromatin condensation leading to the nuclear volume decrease on the early apoptotic stage.

2. Material and methods

2.1. Cell culture, transfection and apoptosis induction

HepG2 cell line stably expressing H4–Dendra2 (obtained from Professor Ivan Raška, Institute of Cellular Biology and Pathology, First Faculty of Medicine, Charles University, Prague, Czech Republic) were cultivated on microscopic 50-mm glass bottom dishes (MatTek, Corporation, Ashland, MA, USA; #P50G-0-30-F) in Dulbecco's modified Eagle's Medium (PAN, Germany) supplemented with 10% fetal calf serum (PAN), 100 IU/ml penicillin, and 100 µg/ml streptomycin in a humidified atmosphere containing 5% CO_2, at 37 °C.

To induce apoptosis cell were treated with etoposide (50 µM)–15 µl per 4 ml of media – right before the real-time microscopic measurements.

2.2. 3D time-lapse live-cell microscopy imaging

Time-lapse live-cell microscopy imaging was performed using Leica TSC SP5 X microscope (Leica, Wetzlar, Germany), equipped with a white-light laser (WLL, 40 mW; Leica, Mannheim, Germany; 470–670 nm in 1 nm increments); 63x/1.40NA oil HCX PL APO lambda blue Objective (Leica) and a 5% CO_2, 37 °C humidified incubation chamber. For scanning WLL was set to 10% of maximal intensity at $\lambda = 490$ nm. 3D scanning of cells (pinhole diameter, 1 Airy; lateral resolution, 0.22 µm; axial resolution, 0.55 µm) and image acquisition were performed in a z-stack time lapse scanning mode using Leica LAS AF software (version 2.1.2). Stacks of 195 *z*-slices (1024×1024 pixels with pixel sizes 102.3 nm × 102.3 nm) were collected at 125.9 nm *z*-spacing and a rate of 2.6 s/slice during 9 h from the moment of cell's treatment with the inductor of apoptosis. Each nucleus occupied less than 140 stacks, therefore it took less than 6 min to obtain every single 3D image of the nucleus.

2.3. Image processing and quantitative image analysis of nuclear apoptotic volume decrease and chromatin condensation

The image processing workflow is demonstrated in Fig. 2 for two nuclei demonstrating no apoptotic morphological features and apoptotic peripheral chromatin condensation, respectively. At the first stage (steps 1–3, Fig. 2A–D) confocal image data analysis is carried out using the freely available ImageJ2 software

(http://imagej.net/ImageJ2). The ImageJ macros (i) provides tracking of single cell nuclei by selection of corresponding ROI at each image sequence (time series), (ii) converts images to gray scale by splitting channels (the green one is selected due to detected fluorescent signal), (iii) corrects for uneven image noise using 3D median filtration with respect to spatial resolution and scan properties, (iv) creates a binary "chromatin" mask by segmentation of an area occupied by chromatin inside a nucleus using a predefined threshold intensity value and “opening” operator for additional morphological noise removal, (v) converts segmented chromatin binary mask to a finite sets of points (*xyz* coordinates) defining chromatin area as an input to the alpha-shape algorithm (Lafarge et al., 2014) to reconstruct the nuclear shape and estimate total nuclear volume, (vi) normalizes image intensity to correct fluorophore photobleaching, typical for time-lapse confocal observations (Pawley, 2010), assuming that cumulative intensity inside the chromatin mask, as well as total chromatin amount inside the nucleus, retains constant value during the whole observation. (vii) Condensed chromatin is detected on image stacks with normalized intensity by chromatin fluorescence intensity exceeding threshold value defined by maximum fluorescence intensity during initial observations when chromatin is assumed to be predominantly in uncondensed state.

Nuclear volume is nearly identical to the overall volume occupied by chromatin when it is uniformly distributed within the nucleus at the early stages of observations. However this is no longer true when early peripheral chromatin condensation begins. To take into account this volume underestimation and accurately measure the observable nuclear volume dynamics we perform reconstruction of the shape of whole nucleus defining it by surface confining the outer boundary of chromatin area. 3D reconstruction of this nuclear surface and nuclear volume estimation is performed by 3d alpha shape algorithm implemented in R package ‘alphashape3d’ (Lafarge et al., 2014) (Fig. 2).

3. Theory and calculation

3.1. Kinetic model of early apoptotic peripheral chromatin condensation and nuclear volume decrease

Kinetic model of peripheral chromatin condensation in the shape of a nuclear shell (so called “apoptotic ring”) proposed here is based on a general mathematical description of the translocation of a specific apoptotic “effector” from the cytoplasm into the nucleus. We do not specify the name of the effector (e.g. AIF) since the detailed molecular mechanism of the chromatin condensation is unknown. However, it is known in the literature that AIF is absent before the condensation and is present during the condensation (Artus et al., 2010; Han et al., 2006; Ho et al., 2006; Scovassi et al., 2009; Ye et al., 2002), therefore the beginning of AIF translocation into the nucleus occurs simultaneously with the beginning of chromatin condensation. Moreover, the concentration of AIF is significantly higher in the area of the condensed chromatin (Artus et al., 2010; Ye et al., 2002) that indicates AIF is bound within the condensed chromatin with a high affinity constant. Therefore, AIF can be a candidate to the role of the apoptotic effector.

In order to mathematically describe the formation dynamics of the intranuclear peripheral shell of the condensed chromatin, we assume the following constrains of the proposed model: (1) the condensed chromatin is located only inside the apoptotic shell, whereas the uncondensed chromatin is located only outside the apoptotic shell in the nuclear (i.e. only the chromatin in the “apoptotic ring” is called “condensed chromatin” in the model); and (2) the concentration of the effector is equal to zero on the inner surface of the shell during the process (to avoid condensation in the center of the nucleus). Then the chromatin condensation occurs only on the inner surface of the shell, and thus the rate of the increase of the condensed chromatin amount (it is proportional to the shell volume) is proportional to the total flux of the effector on the inner surface of the shell (e.g., it is reported in the literature that irreversible binding of chromatin with AIF causes the chromatin condensation (Artus et al., 2010; Sevrioukova, 2011; Vahsen et al., 2006; Ye et al., 2002)).

In addition, we assume that the translocation dynamics of the external apoptotic effector through the nucleus is limited by its intranuclear diffusion through the apoptotic shell. That means the rate of the translocation of the effector through the apoptotic shell is much lower than both (1) the rate of the transport of the effector through the nuclear membrane (that is reasonable due to known fast transport rate of not-large proteins ~60 kDa through the nuclear membrane (Ma et al., 2012; Stewart, 2007; Yang et al., 2004), and AIF and endonuclease G are proteins of such molar mass) and (2) the rate of the chromatin condensation on the inner surface of the apoptotic shell (otherwise, the chromatin would be condensed everywhere inside the nuclear, but not only on the periphery that contradicts with experimental observations). To satisfy such limiting condition the translocation rate of the effector inside the shell should be much slower than in water, – that is possible in the case of a fast reversible binding reaction of the effector with the condensed chromatin (leading to so called “delayed diffusion” of the effector).

It is known in the literature (Kihlmark et al., 2001; Solier and Pommier, 2009, 2014) and also observed in our experiments that the intranuclear peripheral apoptotic shell of the condensed chromatin formed at early apoptosis (our stage I) has rather small thickness in comparison with both the nucleus size and characteristic curvature radius of its surface. This circumstance allows us to apply one-dimensional diffusion equation to describe the translocation dynamics of the effector through the shell of the condensed chromatin.

Therefore, in order to describe stage I, we suggest the following nonstationary (due to stepwise apoptotic dynamics) diffusion equation accompanied by ligand-receptor type reversible binding reaction (inside the shell of the condensed chromatin):

$$\begin{cases} \frac{\partial}{\partial t}G_u = D\frac{\partial^2}{\partial x^2}G_u - k_a(A - G_b)G_u + k_d G_b \\ \frac{\partial}{\partial t}G_b = k_a(A - G_b)G_u - k_d G_b \\ \frac{\partial}{\partial t}A = -k_a(A - G_b)G_u + k_d G_b \end{cases} \quad (1)$$

where x is the coordinate across the apoptotic shell, $G_u = G_u(x,t)$ is the local concentration of the unbound apoptotic effector, D is the diffusion coefficient (assumed to be a constant, i.e. independent of time t and spatial coordinates inside the nucleus), $G_b = G_b(x,t)$ is the local concentration of bound complexes of the effector with condensed chromatin, A is the local concentration of the condensed chromatin binding sites (assumed constant, i.e. independent on t and x inside the shell), k_a is the association rate constant, k_d is the dissociation rate constant. In Eq. (1) we take into account the experimental fact that the diffusion of condensed chromatin is negligible on the time scale of stage I (Fig. 1).

In Eq. (1) we implicitly assume that they are unaffected by the parallel process of decreasing nucleus volume. More specifically, the apoptotic shell deforms elastically keeping its density and, hence, A constant. Then the whole volume change is due to the inner region occupied by uncondensed chromatin and, hence, accompanied by additional change of the concentration of the latter. However, this concentration is anyway irrelevant as long as chromatin condensation is fast enough (limited to the interior of the apoptotic shell). Then Eq. (1) are valid with respect to the moving reference frame (local to the surface element). The outflow of water through the nuclear membrane (and, hence, through the apoptotic shell) in the reverse direction affects only G_u, which we

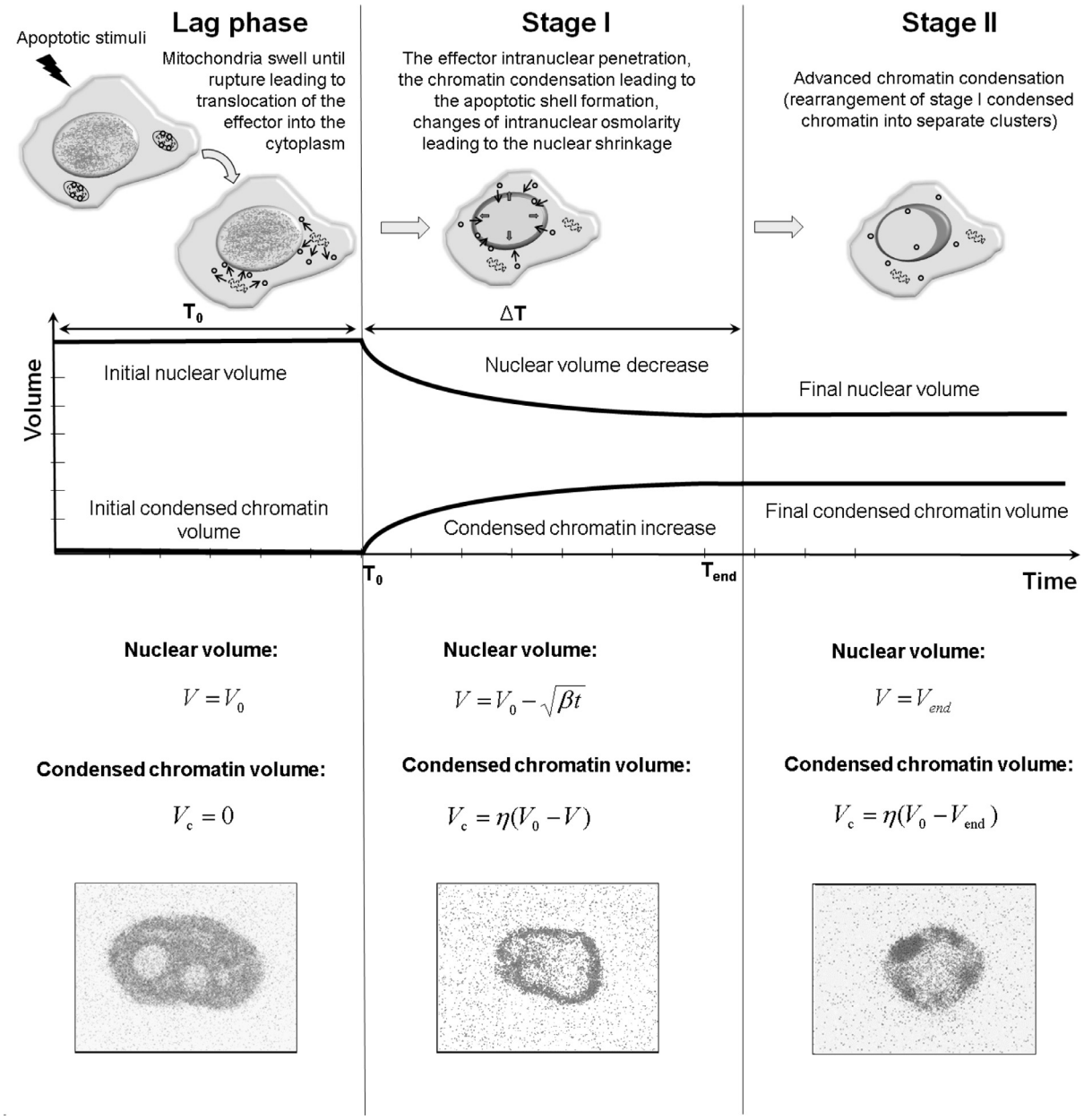

Fig. 1. Model of nuclear apoptotic volume decrease and peripheral chromatin condensation during early stages of nuclear apoptosis. During the lag-phase (*T0*) mitochondria swell until rupture leading to the apoptotic effector translocation from mitochondria into the cytoplasm. On stage I, upon intranuclear penetration the effector initiates chromatin condensation. During this time (ΔT) chromatin gradually condenses against the nuclear periphery forming characteristic shell-like area (so called "apoptotic ring" on 2D pictures). Alterations in chromatin structure result in nuclear volume decrease. By the end of stage I (*Tend*) and beginning of stage II the nucleus volume achieves a final value (*Vend*).

further assume to be negligibly small. We want to emphasize that this model is applicable to a nucleus of arbitrary shape as long as the above assumptions are satisfied. The differential equation for the total concentration of the effector $G = G_u + G_b$ is obtained from Eq. (1) as follows:

$$\frac{\partial}{\partial t}G = D\frac{\partial^2}{\partial x^2}G_u \tag{2}$$

To solve Eqs. (1) and (2) we used the following two assumptions. First, the duration of stage I is much longer than the time of reaching the equilibrium of the reversible binding reaction (between the effector and the chromatin); this assumption is justified by the significantly delayed diffusion, and leads to

$$k_a(A - G_b)G_u - k_d G_b = 0 \tag{3}$$

Second, the concentration of bound complexes is much less than the total concentration of binding (i.e. both bound and unbound) sites in the shell of condensed chromatin:

$$G_b \ll A \tag{4}$$

Assumption (4) is equivalent to the requirement that the concentration of unbound effector G_u is much less than the equilibrium constant $K = k_d/k_a$ of the effector-chromatin binding:

$$G_u \ll K = k_d/k_a \tag{5}$$

In the case of AIF, assumption (5) is supported by known literature experimental data on typical intranuclear total (i.e. both bound and unbound) concentration of AIF (< 3 μg/mL or $< 6{\cdot}10^{-8}$ M (Sun et al., 2017)) (during stage I of apoptosis), which is much less

than the reported equilibrium constant $K=9\cdot10^{-7}$ M (Gong et al., 2007) of reversible binding of AIF with chromatin.

The above two assumptions (3)-(4) lead to the following algebraic relation:

$$G = (1 + k_a A/k_d)G_u \tag{6}$$

Then, Eq. (2) is converted into the form of effective diffusion equation, which we use as a master equation in our model:

$$\frac{\partial}{\partial t}G = \frac{D}{1 + k_a A/k_d}\frac{\partial^2}{\partial x^2}G_u = D_{eff}\frac{\partial^2}{\partial x^2}G \tag{7}$$

Eq. (7) is a reasonable and commonly applicable approach (Orlova et al., 2011), which introduces the effective diffusion coefficient D_{eff} (replacing the intrinsic diffusion coefficient D of G in water) to describe the diffusion delayed (since $D_{eff} < D$) by the binding. In order to solve Eq. (7) we formulated proper boundary conditions presented below.

Let $X(t)$ be x coordinate of the inner surface area of the intranuclear apoptotic shell ($x = 0$ at the outer surface area of the shell), which is the boundary between two phases of the chromatin: condensed and uncondensed ones. The shell inner boundary is moving (i.e. $X(t)$ is increasing) during the chromatin condensation, and the boundary moving rate (dX/dt) depends on the condensed chromatin formation rate (dN_c/dt) as follows:

$$\frac{1}{\rho_c}\frac{dN_c}{dt} = \frac{dV_c}{dt} = \frac{d(SX)}{dt} = S\frac{dX}{dt} + X\frac{dS}{dt} \tag{8}$$

where S is the outer surface area of the shell, ρ_c is the molar density (or concentration) of the condensed chromatin (assumed a constant). The second term ($X \cdot dS/dt$) in the right side of Eq. (8) can be neglected under the following condition, which we assumed in our model:

$$\frac{dX}{dS} \gg \frac{X}{S} \tag{9}$$

In general, the change of the nuclear surface area (during nuclear shrinking) could be explained by the highly folded structure of the nuclear membrane Dahl et al., 2004). Nevertheless, we believe that condition ((9) is a reasonable approximation (which allows to get an analytical solution of master Eq. (7)) in our model, since we found in this work that the shell surface area S reduces slightly while the condensed chromatin volume $V_c = SX$ increases significantly (Fig. 4). That is also supported by known in the literature (Versaevel et al., 2012) and observed in our experiments phenomenon that during chromatin condensation the nucleus rather changes its shape index (becomes more elongated) that allows major change of the volume at minor change of the surface area.

Apoptotic condensation of chromatin takes some amount of the effector, which becomes irreversibly bound with the condensed chromatin (e.g. it is reported in the literature (Vahsen et al., 2006) that chromatin is condensed with the ratio of one AIF molecule to 10 nucleotides), therefore, one can write:

$$N_G = \xi N_c \tag{10}$$

where ξ (assumed to be a constant) is the amount of irreversibly bound effector N_G per unit amount of condensed chromatin N_c. Since there is no effector in the phase of uncondensed chromatin, the amount of the effector irreversibly bound per unit time (i.e. the rate of irreversible binding of the effector with uncondensed chromatin) on the inner surface of the shell should be equal to the diffusion flux of the effector at this boundary:

$$\left.\frac{dN_G}{dt}\right|_{x=X(t)} = -SD_{eff}\left.\frac{\partial G}{dx}\right|_{x=X(t)} \tag{11}$$

Combining Eqs. (8)–(11) we get:

$$\frac{dX}{dt} = -\left.\frac{D_{eff}}{\xi\rho_c}\frac{\partial G}{\partial x}\right|_{x=X(t)} \tag{12}$$

Thus, we get the following moving boundary conditions for master differential Eq. (7):

$$\begin{array}{ll} 0 \le x \le X(t),\ t = 0: & X(0) = 0,\ G(x,0) = 0 \\ x = 0,\ t > 0: & G(0,t) = G_0 \\ x = X(t),\ t > 0: & G(x,t) = 0 \\ x = X(t),\ t > 0: & -\frac{\partial G}{\partial x} = \gamma\frac{dX}{dt} \end{array} \tag{13}$$

where G_0 is the concentration of the effector in cytosol (i.e. on the outer surface of the shell) assumed to be constant (i.e. changed insignificantly) during stage I (in the case of AIF that was experimentally observed in the literature (Sun et al., 2017) and can be theoretically explained by the excess of the total amount of the effector in the cell over the total amount of effector-chromatin bound complexes formed in the nucleus), and γ is the coefficient derived from Eq. (12):

$$\gamma = \frac{\xi\rho_c}{D_{eff}} \tag{14}$$

Partial differential Eq. (7) with moving boundary conditions (13) is known as one-dimensional two-phases Stefan problem (Meirmanov, 1992; Rubinšteĭn, 2000), which fortunately can be solved analytically (Javierre et al., 2006) using a special function, as follows:

$$G(x,t) = G_0\left(1 - \frac{\mathrm{erf}\left(x/\sqrt{4D_{eff}t}\right)}{\mathrm{erf}(\lambda)}\right) \tag{15}$$

$$X(t) = \lambda\sqrt{4D_{eff}t} \tag{16}$$

where erf(y) is the (Gauss) error function:

$$\mathrm{erf}(y) = \frac{1}{\sqrt{\pi}}\int_{-y}^{y} e^{-z^2}dz \tag{17}$$

It follows from Eq. (12) that constant parameter λ in Eq. (15) is determined by the equation

$$\frac{\sqrt{\pi}\gamma D_{eff}}{G_0}\lambda\ \exp(\lambda^2)\ \mathrm{erf}(\lambda) = 1 \tag{18}$$

which can be rewrote taking into account Eq. (14) as follows:

$$\frac{G_0}{\sqrt{\pi}\xi\rho_c} = \lambda\ \exp(\lambda^2)\ \mathrm{erf}(\lambda) \tag{19}$$

Eq. (19) cab be rewrote in a more convenient form (for practical applications) taking into account Eq. (10):

$$\frac{G_c}{G_0} = \frac{1}{\sqrt{\pi}\lambda\ \exp(\lambda^2)\ \mathrm{erf}(\lambda)} = f(\lambda) \tag{20}$$

where $G_c = \xi\rho_c$ is the concentration of irreversibly bound effector in the phase of condensed chromatin. Thus, Eq. (20) establishes the relation between the fraction (G_c/G_0) of irreversibly bound effector and the parameter λ, which determines the condensed chromatin volume as follows from Eq. (16):

$$V_c = SX = S\lambda\sqrt{4D_{eff}t} \tag{21}$$

It is known (Athirasala et al., 2017; Versaevel et al., 2012) that volume (and shape) of interphase nucleus is rather sensitive to the level of chromatin condensation. The condensation of chromatin is characterized by a reduction of volume due to a spatial organization into densely packed higher-order structures (Mora-Bermudez and Ellenberg, 2007). We assumed that the condensed chromatin volume is (approximately) linear proportional to the nuclear volume loss:

$$V_c = \eta(V_0 - V) \tag{22}$$

where the coefficient η is a constant. Obviously, linear Eq. (22) should be applicable up to some (at least rather

small) extent of nuclear deformation. The dependence similar to linear Eq. (22) could be found in literature (Versaevel et al., 2012) for some cells. In our experiments with HepG2 linearity of Eq. (22) was verified in the range of the nuclear volume loss from zero up to 35% of the initial nuclear volume (Figs. 5 and 4).

Taking into account Eq. (22) and the duration T_0 of the lag phase (with the constant nuclear volume V_0) we get from Eq. (21) for the nuclear volume $V(t)$:

$$V(t) = \begin{cases} V_0 & if \quad t < T_0 \\ V_0 - \sqrt{\beta\ (t - T_0)} & if \quad T_0 \le t \le T_{end} \\ V_0 - \sqrt{\beta\ (T_{end} - T_0)} & if \quad t > T_{end} \end{cases} \tag{23}$$

where

$$\beta = \frac{4D_{eff}S^2\lambda^2}{\eta^2} \tag{24}$$

and T_{end} is the time corresponding to the end of the condensation process, when all chromatin condensed and the nucleus volume changed in δ ("shrinking ratio") times and became V_{end}:

$$V_{end} = V_0 - \sqrt{\beta\ (T_{end} - T_0)} = V_0\delta \tag{25}$$

Then the evolution of the condensed chromatin volume is expressed as

$$V_c(t) = \begin{cases} 0 & if \quad t < T_0 \\ \sqrt{\beta\eta^2\ (t - T_0)} & if \quad T_0 \le t \le T_{end} \\ \sqrt{\beta\eta^2 (T_{end} - T_0)} & if \quad t > T_{end} \end{cases} \tag{26}$$

Eqs. (23) and (26) describes the dynamics of stage I of chromatin condensation at the nuclear periphery and corresponding nuclear volume decrease ($T_0 < t < T_{\text{end}}$). The subsequent apoptotic nuclear morphological changes are not accompanied by further chromatin condensation and decrease in nuclear volume that achieves a final constant value $V = V_{\text{end}}$ (stage II, $t > T_{\text{end}}$) and include more advanced rearrangement of condensed chromatin inside the nucleus into separate clusters. With respect to parameters V_0, V_{end}, S_{end}, T_0 and T_{end} the parameter β can be expressed from Eq. (23) as

$$\beta = \frac{(V_0 - V_{end})^2}{\Delta T} \tag{27}$$

$$\Delta T = T_{\text{end}} - T_0 \tag{28}$$

and, therefore, Eq. (23) can be rewritten into the following form, which is convenient for practical applications:

$$V(t) = \begin{cases} V_0 & if \quad t < T_0 \\ V_0 - (V_0 - V_{end})\sqrt{\frac{t}{\Delta T} - \frac{T_0}{\Delta T}} & if \quad T_0 \le t \le T_{end} \\ V_{end} & if \quad t > T_{end} \end{cases} \tag{29}$$

Due to Eq. (22), the volume of the apoptotic shell can be fitted by Eq. (29), as well.

Using Eq. (24) one can evaluate the effective diffusion coefficient D_{eff} of the effector from the obtained $\beta\eta^2$ (or final apoptotic shell volume $V_{c,\,end}$ or thickness X_{end} and duration ΔT of stage I) and S, if λ is known:

$$D_{eff} = \frac{\beta\eta^2}{4S^2\lambda^2} = \frac{V_{c,end}^2}{4S^2\lambda^2\Delta T} = \frac{X_{end}^2}{4\lambda^2\Delta T} \tag{30}$$

According to Eq. (20), required parameter λ can be obtained from the measured fraction G_c/G_0 of irreversibly bound effector (e.g. in particular experiments by labeling the effector with a fluorophore). For example, if the fraction G_c/G_0 is equal to 1, the value of λ is equal to 0.62. Interestingly, the function $f(\lambda)$ in Eq. (20) is changing significantly with λ: the variation of the fraction $G_c/G_0 = f(\lambda)$ in the wide range from 10^{-3} to 10^3 corresponds to the variation of λ in the relatively narrow range from 0.15 to 1.4 (Fig. 3). Therefore, the parameter λ can be evaluated with rather high precision even if the ratio G_c/G_0 is estimated approximately in the range of a few orders of magnitude.

3.2. Characterization of nuclear morphological changes in HepG2 cells treated with etoposide: fitting and statistical analysis

Quantitative assessment of nuclear surface, volume and condensed chromatin changes in HepG2 H4-Dendra2 cells undergoing etoposide-induced apoptosis was obtained using image processing algorithm shown in Fig. 2. Global optimization algorithm DiRect (Jones et al., 1993) implemented in LabView was used to fit the observable dynamics by the developed coupled model of early apoptotic chromatin condensation and nuclear volume decrease and retrieve the model parameters including uncertainties of estimates.

4. Results

Using time-lapse 3D confocal microscopy during 9 h after etoposide treatment we observed the chromatin condensation forming the peripheral nuclear shell (so called "apoptotic ring") at the early apoptosis stage on HepG2 cell line, expressing a fluorescent chromatin marker (histone H4-Dendra2). The observed nuclei reproduced all characteristic signs of early nuclear apoptosis that forced us to suggest the following stages for nuclear morphological changes starting from apoptosis induction time-point: relatively long initial lag-phase, where nucleus preserves its non-apoptotic appearance; fast stage I of peripheral chromatin condensation; and late stage II of the condensed chromatin exhibiting increasing fragmentation into separate beads. Both characteristic features of chromatin changes and transition times agree in part with previously performed in vitro dynamic studies (Tone et al., 2007). Schematically these stages are illustrated in Fig. 1 with basic cellular characteristics and typical 2D slices of corresponding 3D images obtained in this work.

In order to perform the quantitative analysis of observed dynamics of nuclear morphology changes of the cells we applied the developed kinetic model (Fig. 1, Material and Methods). It should be noted that the applicability of the model in processing of experimental kinetics of nuclear alterations depends on cellular characteristics, which can be retrieved from 3D images of cells. To satisfy this requirement we applied the original image-processing algorithm (Fig. 2, Material and Methods) to reconstruct a region occupied by condensed chromatin and the whole nuclear shape at each time point and to quantify dynamics of nuclear volume decrease and chromatin condensation during the whole observation. Finally, we fitted the experimentally measured dynamics of apoptotic volume decrease and peripheral chromatin condensation (the apoptotic shell formation) by Eq. (29) of the proposed model using global optimization (Fig. 4). As a result of this study we determined the following apoptotic characteristics for two analyzed cells: the initial V_0 and the final volumes of the nucleus V_{end} and the condensed chromatin V_c, the lag-phase duration T_0, and the duration ΔT of stage I. These data allow one to evaluate the volume ratio δ, the rate β and the coefficient η of the nuclear shrinkage.

In both cells observations, the nuclear volume loss was ~40%. The prolonged lag-phase of one of the observed cells prevented the detailed description of stage II of nuclear apoptosis (Fig. 4). However clearly visible patterns of condensed chromatin inherent to stage II in the last measured image series confirm that stage I of apoptotic shell formation was observed to the full extent to allow accurate characterization. Demonstrating similar degree of volume decrease and lag-phase duration the cells displayed a significantly different duration of stage I (but both values are within the reported temporal range (Tone et al., 2007)), thus demonstrating

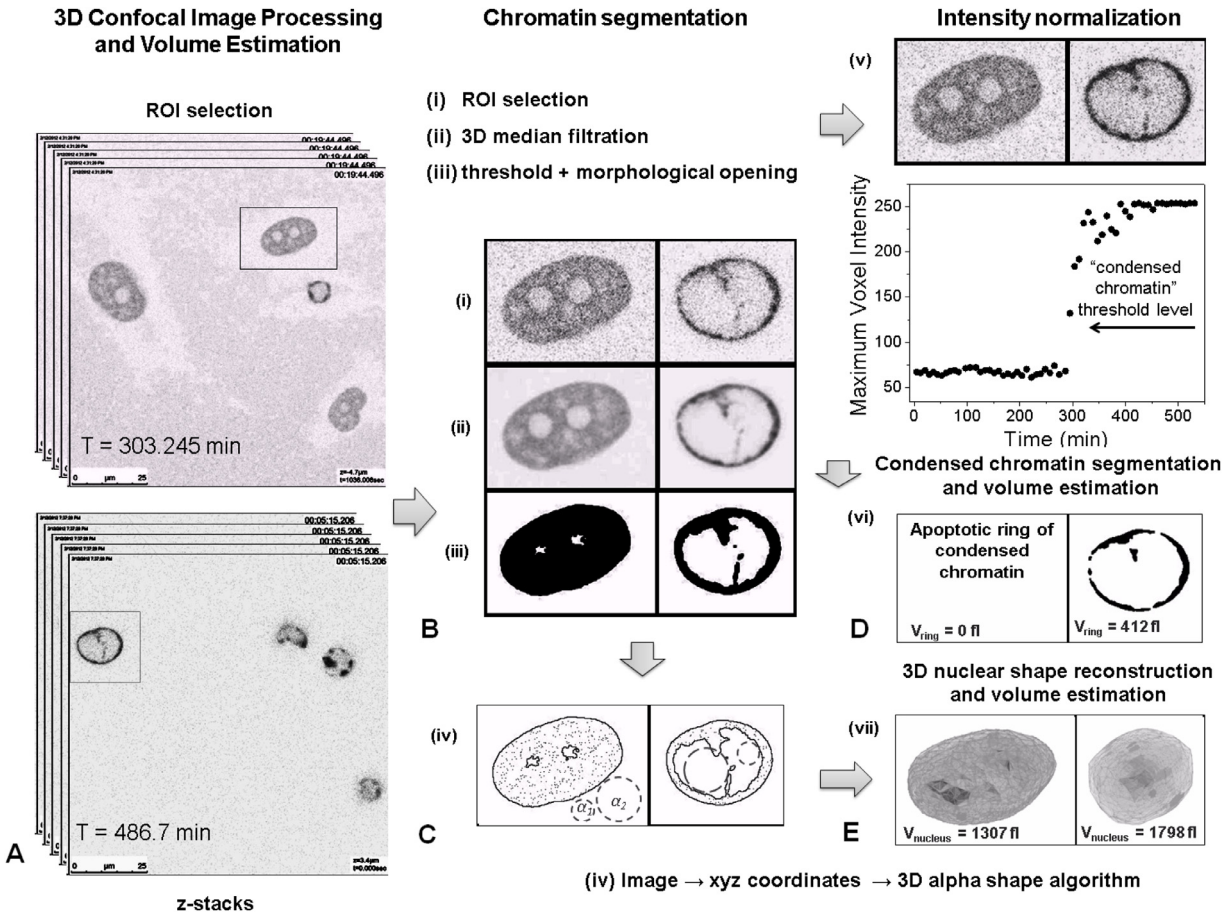

Fig. 2. Image Processing Workflow. (A) Confocal microscopy image data obtained in result of observations is a 4D image stacks (x,y,z,t) organized by time series of z-stack image sequences. The process of 3D confocal image analysis and volumetric estimation of a nucleus and chromatin in condensed state includes following steps: (B) segmentation of an area occupied by chromatin (in both states, e.g. uncondensed and condensed) inside a nucleus; (C) normalization of intensity for image sequences to compensate for fluorophore photobleaching, typical for time-lapse confocal observations; (D) segmentation of an area occupied by chromatin in condensed state and its volume estimation; (E) 3D reconstruction of the whole nuclear shape as a surface bounding chromatin area defined in (B).

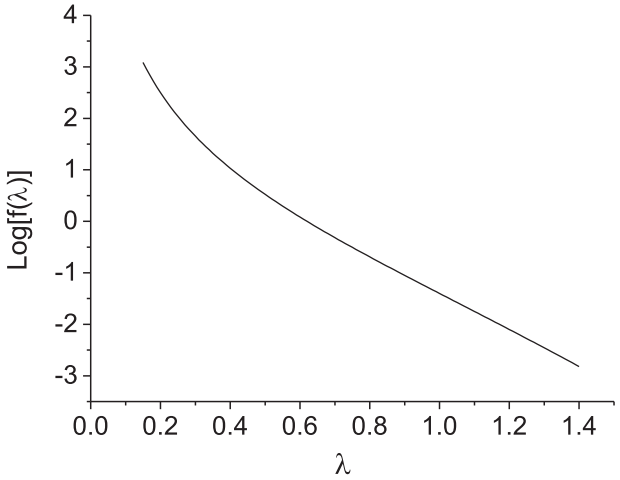

Fig. 3. Decimal logarithm of function $f(\lambda)$ defined by Eq. (20).

cell-to-cell variability (mainly in supposed difference of their mitochondria life-times) in response to chemotherapeutic agent (etoposide).

Independent fitting of the nucleus volumes and the apoptotic shell volume in Fig. 4 by universal Eq. (29) supports one of main statements of the model that chromatin condensation occurs synchronously with the nucleus volume decrease: the lag-phase duration T_0 and the duration ΔT of stage I are equal (in frames of the error) for both volumes. Another important assumption on the approximate conservation of the surface area S during early apoptosis is also supported by our measurements, as shown in Fig. 4. Normalized dependence of the nuclear volume on the condensed chromatin volume (values of V0, Vend and Vc,end are taken from Fig. 4) treated by linear fit in Fig. 5 justifies the important assumption of Eq. (22) used in our model.

5. Discussion

Kinetic model of peripheral chromatin condensation can be interpreted biologically through an apoptotic effector, responsible for initiation of chromatin structure remodeling. Dynamics of chromatin shell formation is limited by the diffusion of the effector through increasing shell of condensed chromatin at the inner face of the nuclear envelope. Particular nature of this effector and its mode of action has not been yet thoroughly studied and completely understood. As mentioned previously, AIF (or endonuclease G, or both) may initiate early chromatin condensation upon its nuclear translocation and change chromatin structure as a result of direct binding to DNA (Loo et al., 2002; Ye et al., 2002) or forming remodeling complexes in cooperation with other nuclear proteins (e.g. histone protein γH2AX (Baritaud et al., 2010)). In order to finally elucidate this issue additional experimental evidence might be obtained by incorporating other fluorescent readouts. However,

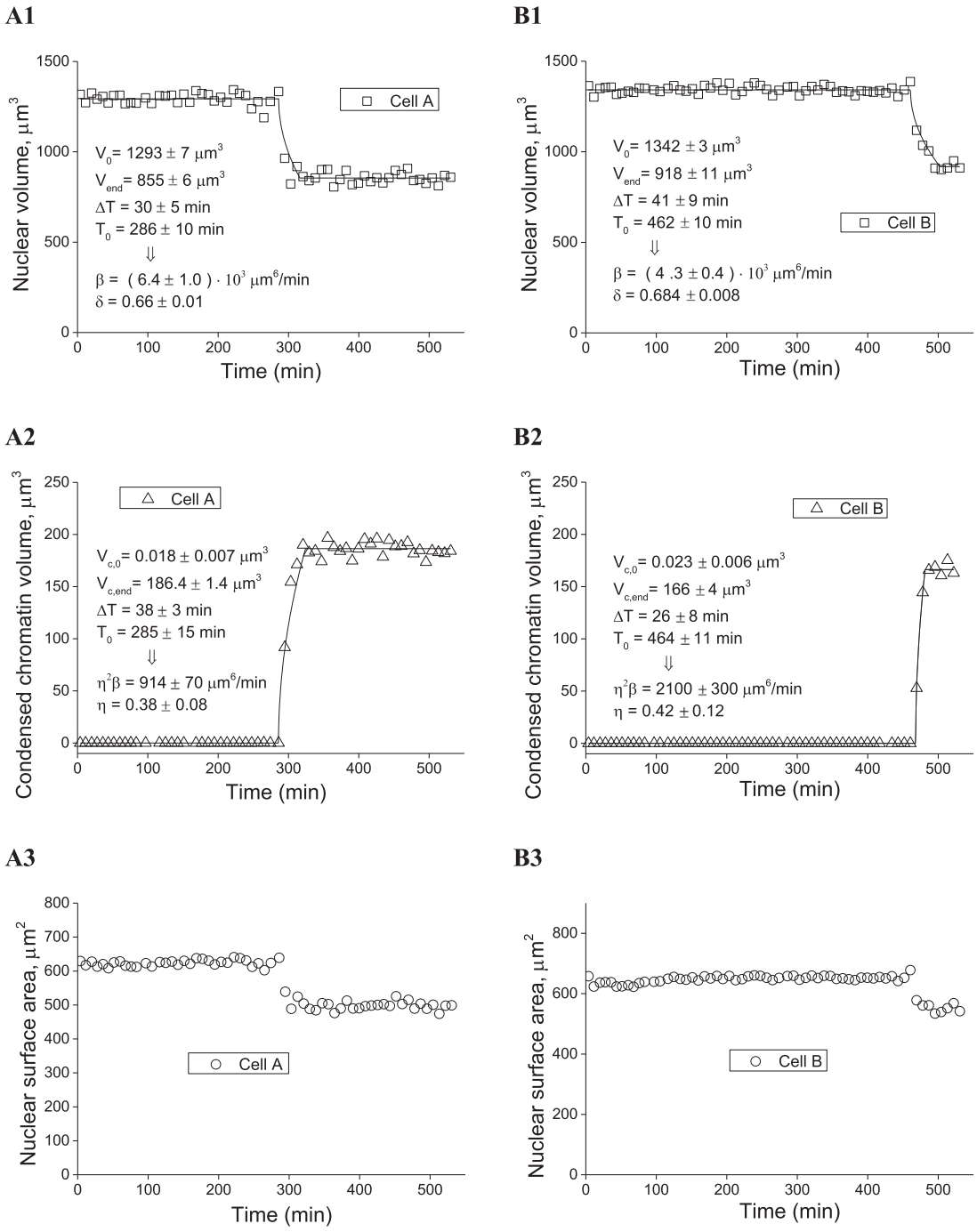

Fig. 4. Dynamics of individual HepG2 cells undergoing etoposide-induced apoptosis: the nuclear volume (squares), the condensed chromatin volume (triangles) and the nuclear surface area (circles) of two tracked cells, fitted by the model presented in Eq. (29).

the nature and intranuclear activity of hypothesized effector can also be evaluated indirectly from dynamic characteristics provided by the model, including lag-phase duration related to the time required for effector activation in the cytoplasm, and the rate and duration of stage I chromatin condensation related to the particular mechanism of effector's action.

Whereas dynamics of chromatin condensation reflects biochemical aspects of apoptosis, we assume that nature of nuclear shrinkage is predominantly physicochemical. An immediate corollary of this model is direct interrelation between dynamics of nuclear shrinkage and chromatin condensation, which calls for simultaneous observation of dynamics of these processes.

Experimental observation of nuclear volume decrease simultaneous to chromatin condensation (Fig. 4) is consistent to our assumption of underlying mechanism. Thus, our approach does not only provide direct experimental evidence of the connection between these two inherent apoptotic features, but also supports it by quantitative evaluation. The apparent contradiction to previously reported shrinkage beginning during stage II (Tone et al., 2007) is likely related to abovementioned differences in the interpretation of term "shrinkage". While we consider overall nuclear volume decrease supported by its direct measurement, the other study operates "nuclear shrinkage" as overall compaction of the chromatin related to its relative density.

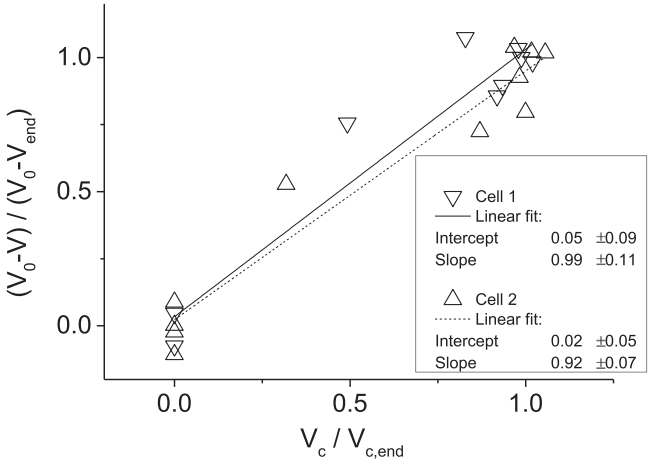

Fig. 5. Normalized dependence of the nuclear volume on the condensed chromatin volume (values of V0, Vend and Vc,end *are* taken *from* Fig. 4) treated by linear fit according to Eq. (22).

The nuclei lost their volume during stage I of chromatin condensation and there is no subsequent volume decrease during stage II (Fig. 4). Under proposed kinetic model of nuclear shrinkage, this implies that the most considerable chromatin structure remodeling takes place during stage I of peripheral chromatin condensation. By contrast, during stage II chromatin undergoes conformational changes only on macro level, i.e. peripheral areas of completely condensed chromatin are organized into compact irregular separated clusters, to be further packed into apoptotic bodies at the final stages of apoptosis.

In conclusion, we studied dynamics of nuclear apoptosis based on detailed analysis of its inherent morphological features, including nuclear shrinkage and chromatin condensation. To process time-lapse 3D confocal microscope images we developed: (1) combined mathematical model of early nuclear apoptosis, incorporating peripheral chromatin condensation and nuclear volume decrease and (2) image processing algorithm for quantitative measurement of volumes of the whole nucleus and of the condensed chromatin as functions of time. This enabled detailed characterization of the observed processes by their lag-phase duration, entry times into stage I and stage II of nuclear apoptosis, rate and degrees of nuclear shrinkage (volume decrease) and chromatin condensation. The method is intended for enhanced investigation of early stages of nuclear apoptosis, their morphological appearance, and underlying mechanisms, which is essential for understanding their role in apoptotic death program and searching for possible ways to regulate the latter. Quantitative characterization of apoptotic volume decrease opens a way for direct comparison of results of apoptosis studies performed in different laboratories.

Acknowledgments

Experimental work was supported by the Czech Science Foundation (grant P302-12-G157) to provide confocal microscopy of cells. Theoretical work was supported by Russian Foundation for Basic Research (grant 16-04-01283) and Russian Science Foundation (grant 17-75-20117).

References

Allera, C., Lazzarini, G., Patrone, E., Alberti, I., Barboro, P., Sanna, P., Melchiori, A., Parodi, S., Balbi, C., 1997. The condensation of chromatin in apoptotic thymocytes shows a specific structural change. J. Biol. Chem. 272, 10817–10822.

Artus, C., Boujrad, H., Bouharrour, A., Brunelle, M.-N., Hoos, S., Yuste, V.J., Lenormand, P., Rousselle, J.-C., Namane, A., England, P., Lorenzo, H.K., Susin, S.A., 2010. AIF promotes chromatinolysis and caspaseindependent programmed necrosis by interacting with histone H2AX. EMBO J 29, 1585–1599.

Athirasala, A., Hirsch, N., Buxboim, A., 2017. Nuclear mechanotransduction: sensing the force from within. Curr. Opin. Cell Biol. 46, 119–127.

Baritaud, M., Boujrad, H., Lorenzo, H.K., Krantic, S., Susin, S.A., 2010. Histone H2AX: the missing link in AIF-mediated caspase-independent programmed necrosis. Cell Cycle 9, 3186–3193.

Bhola, P.D., Mattheyses, A.L., Simon, S.M., 2009. Spatial and temporal dynamics of mitochondrial membrane permeability waves during apoptosis. Biophys. J. 97, 2222–2231.

Candé, C., Vahsen, N., Garrido, C., Kroemer, G., 2004. Apoptosis-inducing factor (AIF): caspase-independent after all. Cell Death Differ 11, 591–595.

Candé, C., Cohen, I., Daugas, E., Ravagnan, L., Larochette, N., Zamzami, N., Kroemer, G., 2002. Apoptosis-inducing factor (AIF): a novel caspase-independent death effector released from mitochondria. Biochimie 84, 215–222.

Dahl, K.N., Kahn, S.M., Wilson, K.L., Discher, D.E., 2004. The nuclear envelope lamina network has elasticity and a compressibility limit suggestive of a molecular shock absorber. J. Cell Sci. 117, 4779–4786.

Gong, M., Hay, S., Marshall, K.R., Munro, A.W., Scrutton, N.S., 2007. DNA binding suppresses human AIF-M2 activity and provides a connection between redox chemistry, reactive oxygen species, and apoptosis. J. Biol. Chem. 282, 30331–30340.

Han, W., Shi, X., Nuttall, A.L., 2006. AIF and endoG translocation in noise exposure induced hair cell death. Hearing Res. 211, 85–95.

Hangen, E., Blomgren, K., Bénit, P., Kroemer, G., Modjtahedi, N., 2010. Life with or without AIF. Trends Biochem. Sci 35, 278–287.

Hangen, E., raud, O.F., Lachkar, S., Mou, H., Doti, N., Fimia, G.M., Lam, N., Zhu, C., Godin, I., Muller, K., Chatzi, A., Nuebel, E., Ciccosanti, F., Flamant, S., nit, P.B., Perfettini, J.-L., Sauvat, A., Bennaceur-Griscelli, A., Roux, K.S.-L., Gonin, P., Tokatlidis, K., Rustin, P., Piacentini, M., Ruvo, M., Blomgren, K., Kroemer, G., Modjtahedi, N., 2015. Interaction between AIF and CHCHD4 regulates respiratory chain biogenesis. Mol. Cell 58, 1001–1014.

Hendzel, M.J., Nishioka, W.K., Raymond, Y., Allis, C.D., Bazett-Jones, D.P., Th'ng, J.P.H., 1998. Chromatin condensation is not associated with apoptosis. J. Biol. Chem. 273, 24470–24478.

Ho, T.-C., Yang, Y.-C., Cheng, H.-C., Wu, A.-C., Chen, S.-L., Chen, H.-K., Tsao, Y.-P., 2006. Activation of mitogen-activated protein kinases is essential for hydrogen peroxide -induced apoptosis in retinal pigment epithelial cells. Apoptosis 11, 1899–1908.

Javierre, E., Vuik, C., Vermolen, F.J., Zwaag, S.v.d., 2006. A comparison of numerical models for one-dimensional Stefan problems. J. Comp. Appl. Math. 192, 445–459.

Jones, D.R., Perttunen, C.D., Stuckman, B.E., 1993. Lipschitzian optimization without the Lipschitz constant. J. Optim. Theory Appl. 79, 157–181.

Joza, N., Pospisilik, J.A., Hangen, E., Hanada, T., Modjtahedi, N., Penninger, J.M., Kroemera, G., 2009. AIF: not Just an Apoptosis-Inducing Factor. Ann. N.Y. Acad. Sci. 1171, 2–11.

Kerr, J.F.R., Wyllie, A.H., Currie, A.R., 1972. Apoptosis: A basic biological phenomenon with wideranging implications in tissue kinetics. Br. J. Cancer 26, 239–257.

Kihlmark, M., Imreh, G., Hallberg, E., 2001. Sequential degradation of proteins from the nuclear envelope during apoptosis. J. Cell Sci. 114, 3643–3653.

Lafarge, T., Pateiro-López, B., Possolo, A., Dunkers, J.P., 2014. R implementation of a polyhedral approximation to a 3D set of points using the α-shape. J. Stat. Softw. 56, 1–19.

Li, L.Y., Luo, X., Wang, X., 2001. Endonuclease G is an apoptotic DNase when released from mitochondria. Nature 412, 95–99.

Loo, G.v., Saelens, X., Gurp, M.v., MacFarlane, M., Martin, S.J., Vandenabeele, P., 2002. The role of mitochondrial factors in apoptosis: a Russian roulette with more than one bullet. Cell Death Differ. 9, 1031–1042.

Ma, J., Goryaynov, A., Sarma, A., Yang, W., 2012. Self-regulated viscous channel in the nuclear pore complex. PNAS 109, 7326–7331.

Martelli, A.M., Zweyer, M., Ochs, R.L., Tazzari, P.L., Tabellini, G., Narducci, P., Bortul, R., 2001. Nuclear apoptotic changes: an overview. J. Cell. Biochem. 82, 634–646.

Maté, M.J., Ortiz-Lombardía, M., Boitel, B., Haouz, A., Tello, D., Susin, S.A., Penninger, J., Kroemer, G., Alzari, P.M., 2002. The crystal structure of the mouse apoptosis-inducing factor AIF. Nat. Struct. Biol. 9, 442–446.

Meirmanov, A.M., 1992. The Stefan Problem. Walter de Gruyter, New York.

Mora-Bermudez, F., Ellenberg, J., 2007. Measuring structural dynamics of chromosomes in living cells by fluorescence microscopy. Methods 41, 158–167.

Oberhammer, F., Wilson, J.W., Dive, C., Morris, I.D., Hickman, J.A., Wakeling, A.E., Walker, P.R., Sikorska, M., 1993. Apoptotic death in epithelial cells: cleavage of DNA to 300 and/or 50 kb fragments prior to or in the absence of internucleosomal fragmentation. EMBO J 12, 3679–3684.

Orlova, D.Y., Bártová, E., Maltsev, V.P., Kozubek, S., Chernyshev, A.V., 2011. A nonfitting method using a spatial sine window transform for inhomogeneous effective diffusion measurements by FRAP. Biophys. J. 100, 507–516.

Pantic, I., Harhaji-Trajkovic, L., Pantovic, A., Milosevic, N., Trajkovic, V., 2012. Changes infractal dimension and lacunarity as early markers of UV-induced apoptosis. J. Theor. Biol. 303, 87–92.

Patterson, G.H., Knobel, S.M., Sharif, W.D., Kain, S.R., Piston, D.W., 1997. Use of the green fluorescent protein and its mutants in quantitative fluorescence microscopy. Biophys. J. 73, 2782–2790.

Pawley, J., 2010. Handbook of Biological Confocal Microscopy. Springer Science & Business Media.

Robertson, J.D., Orrenius, S., Zhivotovsky, B., 2000. Review: nuclear events in apoptosis. J. Struct. Biol. 129, 346–358.

Rubinšteĭn, L.I., 2000. Translations of mathematical monographs The Stefan problem. Am. Math. Soc. 27, 419.
Samejima, K., Earnshaw, W.C., 2005. Trashing the genome: the role of nucleases during apoptosis. Nat. Rev. Mol. Cell Biol. 6, 677–688.
Saraste, A., Pulkki, K., 2000. Morphologic and biochemical hallmarks of apoptosis. Cardiovasc. Res. 45, 528–537.
Scovassi, A.I., Soldani, C., Veneroni, P., Bottone, M.G., Pellicciarib, C., 2009. Changes of mitochondria and relocation of the apoptosis inducing factor during apoptosis. Ann. N.Y. Acad. Sci. 1171, 12–17.
Sesso, A., Belizario, J.E., Marques, M.M., Higuchi, M.L., Schumacher, R.I., Colquhoun, A., Ito, E., Kawakami, J., 2012. Mitochondrial swelling and incipient outer membrane rupture in preapoptotic and apoptotic cells. Anat. Rec. 295, 1647–1659.
Sevrioukova, I.F., 2011. Apoptosis-inducing factor: structure, function, and redox regulation. Antioxid Redox Signal 14, 2545–2579.
Solier, S., Pommier, Y., 2009. The apoptotic ring: a novel entity with phosphorylated histones H2AX and H2B and activated DNA damage response kinases. Cell Cycle 8, 1853–1859.
Solier, S., Pommier, Y., 2014. The nuclear γ-H2AX apoptotic ring: implications for cancers and autoimmune diseases. Cell. Mol. Life Sci. 71, 2289–2297.
Stewart, M., 2007. Molecular mechanism of the nuclear protein import cycle. Nat. Rev. Mol. Cell Biol. 8, 195–208.
Sun, M.G., Williams, J., Munoz-Pinedo, C., Perkins, G.A., Brown, J.M., Ellisman, M.H., Green, D.R., Frey, T.G., 2007. Correlated three-dimensional light and electron microscopy reveals transformation of mitochondria during apoptosis. Nat. Cell Biol. 9, 1057–1065.
Sun, Y., Gao, W., Zhao, Y., Cao, W., Liu, Z., Cui, G., Tong, L., Lei, F., Tang, B., 2017. Visualization and inhibition of mitochondria-nuclear translocation of apoptosis inducing factor by a graphene oxide-DNA nanosensor. Anal. Chem. 89, 4642–4647.
Susin, S.A., Daugas, E., Ravagnan, L., Samejima, K., Zamzami, N., Loeffler, M., Costantini, P., Ferri, K.F., Irinopoulou, T., Prévost, M.-C., Brothers, G., Mak, T.W., Penninger, J., Earnshaw, W.C., Kroemer, G., 2000. Two distinct pathways leading to nuclear apoptosis. J. Exp. Med. 192, 571–580.
Susin, S.A., Lorenzo, H.K., Zamzami, N., Marzo, I., Snow, B.E., Brothers, G.M., Mangion, J., Jacotot, E., Costantini, P., Loeffler, M., Larochette, N., Goodlett, D.R., Aebersold, R., Siderovski, D.P., Penninger, J.M., Kroemer, G., 1999. Molecular characterization of mitochondrial apoptosis-inducing factor. Nature 397, 441–446.
Tone, S., Sugimoto, K., Tanda, K., Suda, T., Uehira, K., Kanouchi, H., Samejima, K., Minatogawa, Y., Earnshaw, W.C., 2007. Three distinct stages of apoptotic nuclear condensation revealed by time-lapse imaging, biochemical and electron microscopy analysis of cell-free apoptosis. Exp. Cell Res. 313, 3635–3644.
Vahsen, N., Cande, C., Dupaigne, P., Giordanetto, F., Kroemer, R.T., Herker, E., Scholz, S., Modjtahedi, N., Madeo, F., Cam, E.L., Kroemer, G., 2006. Physical interaction of apoptosis-inducing factor with DNA and RNA. Oncogene 25, 1763–1774.
Versaevel, M., Grevesse, T., Gabriele, S., 2012. Spatial coordination between cell and nuclear shape within micropatterned endothelial cells. Nat. Commun. 671 (3), 1–11.
Widlak, P., Palyvoda, O., Kumala, S., Garrard, W.T., 2002. Modeling apoptotic chromatin condensation in normal cell nuclei requirement for intranuclear mobility and actin involvement. J. Biol. Chem. 277, 21683–21690.
Williams, J.R., Little, J.B., Shipley, W.U., 1974. Association of mammalian cell death with a specific endonucleolytic degradation of DNA. Nature 252, 754–755.
Willingham, M.C., 1999. Cytochemical Methods for the Detection of Apoptosis. J. Histochem. Cytochem. 47, 1101–1109.
Wyllie, A.H., Kerr, J.F., Currie, A.R., 1980. Cell death: the significance of apoptosis. Int. Rev. Cytol. 68, 251–306.
Yang, W., Gelles, J., Musser, S.M., 2004. Imaging of single-molecule translocation through nuclear pore complexes. PNAS 101, 12887–12892.
Ye, H., Cande, C., Stephanou, N.C., Jiang, S., Gurbuxani, S., Larochette, N., Daugas, E., Garrido, C., Kroemer, G., Wu, H., 2002. DNA binding is required for the apoptogenic action of apoptosis inducing factor. Nat. Struct. Mol. Biol. 9, 680–684.
Yuste, V.J., Sánchez-López, I., Solé, C., Moubarak, R.S., Bayascas, J.R., Dolcet, X., Encinas, M., Susin, S.A., Comella, J.X., 2005. The Contribution of apoptosis-inducing factor, caspase-activated DNase, and inhibitor of caspase-activated DNase to the nuclear phenotype and DNA degradation during apoptosis. J. Biol. Chem. 280, 35670–35683.